JME

Journal of Mining & Environment,
Vol.5, No.2, 2014, 67-77.

AN-EUL method for automatic interpretation of potential field data in unexploded ordnances (UXO) detection

M. Abedi[1]*, K. Mosazadeh[2], H. Dehghani[2], A. MadanchiZare[2]

1. Department of Mining Engineering, College of Engineering, University of Tehran, Tehran, Iran
2. Malek Ashtar University of Technology, Tehran, Iran

Received 3 Septebmer 2013; received in revised form 27 August 2014; accepted 6 Septebmer 2014
**Corresponding author: maysamabedi@ut.ac.ir (M. Abedi)*

Abstract

This study applied an automatic interpretation method of potential field data called AN-EUL in unexploded ordnance (UXO) prospect, which is indeed a combination of the analytic signal and the Euler deconvolution approaches. The method can be applied for both magnetic and gravity data as well for their gradient surveys based upon the concept of the structural index (SI) of a potential field anomaly, which is related to the geometry of the anomaly sources. With AN-EUL method, both the depth and the approximate geometry (or SI) of the causative sources can be deduced. A realistic model for UXO to be simulated by a simple shape body is a prolate spheroid. The AN-EUL method is applied to synthetic potential field data (gravity and magnetic) by simulation of a collection of causative sources replicating various UXO sizes placed at different depths. In both cases, the estimated depth and the SI of the synthetic UXOs approximately correspond to the synthetic model parameters. The location detection of the causative sources is based upon the Blakely automatic picking algorithm. For both data sets, since the anomaly responses of the small UXOs are affected by noise, the estimated SI is a bit disturbed but the locations correspond to the real ones. The Blakely algorithm also identifies weak anomalies that are due to noise in data; thus, post-processing of the estimated SI of the automatically detected sources may be needed to prevent false alarm sources in UXO exploration. Two field data sets were provided to demonstrate the capability of the applied methods in UXO detection.

Keywords: *Potential Field Data, UXO Detection, AN-EUL Method, Blakely Algorithm, Automatic Interpretation.*

1. Introduction

Shallow geophysical imaging methods are increasingly implemented in anomaly mapping of buried objects on both land and underwater. Geophysical explorations are vastly superior to the traditional surveys as they minimize drastically time, danger and cost factors [1-2]. One of the main buried objects the investigation of which is underway to develop appropriate geophysical approaches is the unexploded ordnance (UXO).

The aim of UXO cleanup over large contaminated territories is a sophisticated process at all military areas. In many cases, the prospected UXO are routinely detected by sensor sweeps (metal detectors) or geophysical surveys, relative to the background of the region of interest (geologic background and cultural clutter). Geophysical anomalies of UXO bodies result from the contrast in physical properties related to the host medium materials. Localized geological features and other buried cultural objects (comprising of noise objects in UXO detection such as ordnance scrap, cans, wire, etc.) also yield physical property contrasts and subsequently cause undesirable geophysical anomalies. Since in many geological conditions, physical property contrasts between UXO and geological settings (soil and rock) are large, UXO detection is a straightforward process.

The major problem in geophysical-based UXO detection is the existence of false alarms produced by noise objects, which needs the discrimination algorithms in order to distinguish between varieties of anomaly sources. However, there is no general capability to discriminate UXO geophysical anomalies from false alarm anomalies effectively. It has been noted that for carefully executed geophysical surveys, the probability of UXO detection on documented test sites can exceed 90%. However, the false alarm rate of non-UXO targets excavated against each detected UXO remains quite high. Without discrimination capability between different causative sources, large numbers of false alarm anomalies must be considered as potential UXO sources, with approximately 75% of the cleanup cost spent on project [3-4].

The widespread geophysical methods for UXO detection are total field magnetometers (TFM) and time domain electromagnetic induction (TDEM) [5-11]. Application of these methods by experienced geophysical practitioners during demonstrations at controlled UXO test sites achieves probabilities of detection of UXO in excess of 90% (e.g. [12]). Other geophysical methods which are worth less in UXO detection consist of ground penetrating radar (GPR), frequency domain electromagnetic induction (FDEM) systems, multi-gate TDEM systems, multi-component TDEM systems, multi-component (vector) magnetometers, magnetic gradiometers, gravimetry, and their airborne systems [4] and [13-26]. The TFM and TDEM surveys from a helicopter platform at 1-2 m sensor elevation have shown promise for covering large area under UXO detection. Multi-gate (25–30 time gates), multi-component TDEM systems and multi-frequency FDEM systems have also valuable potential for UXO detection [27-30].

The potential field methods (gravity and magnetic) are among the most effective geophysical techniques for UXO detection [21, 22], especially the use of magnetic and magnetic gradiometer methods for both ground-based and airborne surveys has been extensively studied [9, 31, 32]. Therefore, using an automatic method to interpret UXO anomalies in potential field data can be effective. The AN-EUL approach as a previously developed method in mineral exploration (e.g. [33]) can be a straightforward method in the interpretation of UXO anomalies. The applied approach uses the derivatives of potential field data on which a combination of the analytic signal and the Euler deconvolution methods are based. Both the depth and the structural index (SI) of the sources can be automatically estimated by AN-EUL method. Moreover, before applying the AN-EUL method, the Blakely algorithm is also used to detect the locations of the probable UXO targets automatically [34]. Since the majority of UXO targets are similar to a prolate spheroid, we assume such simple shape to simulate the UXO in this study. Both the depth and the shape of a potential source are simultaneously determined at the location of maxima of the analytic signal output which can be selected automatically as the location of causative source using the Blakely algorithm. In what follows, the utility and the applicability of the methods are examined for both synthetic and real data in potential field exploration.

2. Methodology

To describe formulation of the AN-EUL method concisely, we need to explain the analytic signal and the Euler method which are combined to generate simultaneously equations of the depth and the SI. The complex analytic signal [35-37] can be defined as the horizontal and vertical derivatives of the potential field data as follow,

$$A(x,y) = (\frac{\partial P}{\partial x}\hat{x} + \frac{\partial P}{\partial y}\hat{y} + i\,\frac{\partial P}{\partial z}\hat{z}) \tag{1}$$

where $\hat{x}, \hat{y}$ and $\hat{z}$ are unit vectors in the x, y and z directions, i is the imaginary number $\sqrt{-1}$, $\partial P/\partial z$ is the vertical and $\partial P/\partial x$ and $\partial P/\partial y$ are the horizontal derivatives of the potential field data. The 3D calculation of the amplitude of the analytic signal (AAS) is,

$$|AAS(x,y)| = \sqrt{(\frac{\partial P}{\partial x})^2 + (\frac{\partial P}{\partial y})^2 + (\frac{\partial P}{\partial z})^2} \tag{2}$$

The amplitude of the nth-order derivative analytic signal is as follows,

$$|AAS_n(x,y)| = \sqrt{(\frac{\partial P_n^z}{\partial x})^2 + (\frac{\partial P_n^z}{\partial y})^2 + (\frac{\partial P_n^z}{\partial z})^2} \tag{3}$$

where the superscript z denotes the vertical derivative of potential field data. The horizontal derivative can be simply calculated using finite difference method or fast Fourier transform (FFT). The Hilbert transform in frequency domain can be used to calculate the vertical derivative as well [9, 33, 38-40].

Euler deconvolution of potential field data is a well-known interpretation technique, which uses the derivatives of observed data in order to estimate the depth to the top of a causative magnetic or gravity source. The utility of Euler deconvolution method has been well presented in Reid (1995) while Thompson (1982) developed the approach and applied it along profile data, then, Reid et al. (1990) followed up a suggestion in Thompson's work and developed the extension to gridded potential field data [41-43]. Here we briefly discuss the formulation of the Euler method. Any 3D potential function $P(x,y,z)$ is said to be homogenous of degree *n* if the function obeys the following Equation,

$$P(tx,ty,tz)=t^{n}P(x,y,z) \tag{4}$$

Then by differentiating Eq. (4) with respect to *t*, it can be shown that,

$$(x-x_0)\frac{\partial P}{\partial x}+(y-y_0)\frac{\partial P}{\partial y}+(z-z_0)\frac{\partial P}{\partial z}=N\,(\mathrm{B-P}) \tag{5}$$

where (x_0,y_0,z_0) is the position of a potential source whose field is measured at (x,y,z). The potential field has a regional background value of *B*. Note that *N* (or SI) corresponds to –*n* in Euler's Eq. (5) [9, 33, 39, 43-45].

Taking the derivatives in the *x*, *y* and *z* directions of both Euler's Eq. (5) and as well its first vertical derivative and setting $x=x_0, y=y_0$ and $z=0$, we get the depth and the SI at the center of the source as follow,

$$z_0=\left(\frac{|AAS_1||AAS_0|}{|AAS_2||AAS_0|-|AAS_1|^2}\right)_{x=x_0,\mathrm{y=y_0}} \tag{6}$$

$$N=\left(\frac{2|AAS_1|^2-|AAS_2||AAS_0|}{|AAS_2||AAS_0|-|AAS_1|^2}\right)_{x=x_0,\mathrm{y=y_0}} \tag{7}$$

Equations (6) and (7) show that both the SI (which indicates the geometry of the source) and the depth of a potential field anomaly can be simultaneously calculated from the *AAS* and its first- and second-order derivatives at the center of potential source [33].

The SI shows how fast the potential field decreases as a function of distance to the source. For instance in magnetic anomaly, the SI of some simple bodies such as sphere, cylinder/pipe, sill/thin dyke, thick step and contact are 3, 2, 1, 0.5 and 0, respectively. The same holds true for magnetic gradient anomalies as the SI of these shapes are 4, 3, 2, 1.5 and 1, respectively (because of the first-order derivative of magnetic data, the SI increases one unit in the gradient data). Subtracting one unit from SI of both magnetic and its gradient, the SI of gravity and its gradient would be produced for aforementioned simple bodies [42, 43]. Since UXO sources are assumed to be simulated by a prolate spheroid, the SI of such body has a value between the SI of cylinder and sphere models. Therefore, it is at interval (2 to 3) in magnetic anomaly and at (1 to 2) for gravity. The gradient values also locate at (3 to 4) and (2 to 3) respectively for magnetic and gravity sources.

Having calculated the analytic signal of noise-removed potential field data (preprocessed data), the Blakely algorithm [34] is used to automatically find peaks in the grid to determine the locations of probable UXOs. The AN-EUL method estimates the SI and the depth of UXOs at locations picked by the Blakely algorithm. The Blakely test analyzes these peaks in up to 4 directions (along the raw, along the column and along both diagonals) for 8 nearest grid cells. If the grid cell being examined has a higher value than those do on all directions, it is selected as a probable target in analytic signal map. This algorithm indeed will select picks of analytic signal map by scanning all grid cells using a 3×3 pixels window. The depth and the SI of this target subsequently were estimated using the AN-EUL method and then selected as a UXO target provided that has a SI at the desired interval (post processing stage shown in Figure 1). Otherwise, it is assumed as a scrap or non-UXO target.

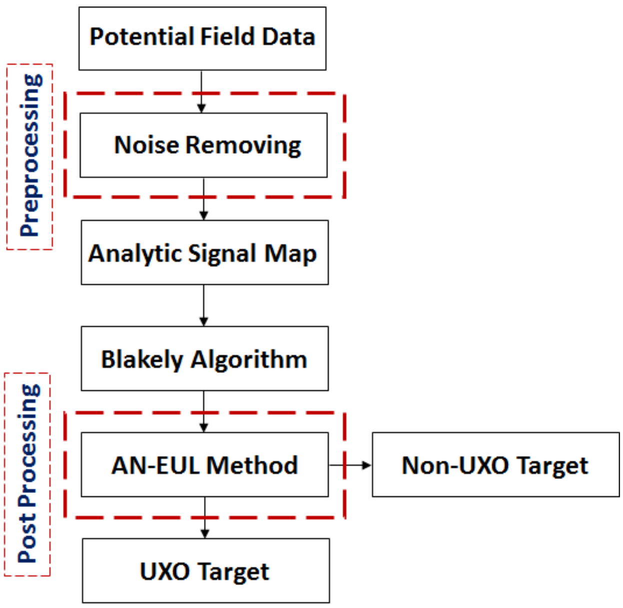

Figure 1. Algorithm of automatic UXO detection using the Blakely algorithm and the AN-EUL method.

3. Synthetic modeling

A set of synthetic prolate spheroid bodies to simulate UXO sources has been assumed in this study. Then the capability of the AN-EUL method in determination of geometry (SI) and depth of picked anomalies by the Blakely algorithm was evaluated. Table 1 presents the parameters of 16 ordnance items which were assumed to simulate the UXOs with a simple shape body, i.e. the prolate spheroid. Varieties of causative sources by changing value of azimuth and plunge of the prolate spheroid were generated to simulate a real case study. Figure 2 shows the geometry of a synthetic model in this study. The location and distribution of assumed bodies have been indicated in Figure 3 in 2D and 3D plots. We attempted to model ordnance items with similar dimensions of the synthetic prolate spheroid in Table 1. Gravity and magnetic anomalies from the samples are presented in Figure 4a and b, respectively.

Table 1. Synthetic parameter sets for ordnance item models shown in Figure 2.

Obj. Num.	Ordnance item	Length (m)	Diameter (m)	Volume (m^3)	Bulk density (gr/cm^3)	Sus. (SI)	X Cor. (m)	Y Cor. (m)	Depth (m)	Azimuth	Plunge
1	40mm Grenade	0.0775	0.0425	0.000073	3	260	12	17	0.06	150	0
2	Hand Grenade	0.1110	0.0630	0.000231	3.5	260	14	12	0.09	30	125
3	57mm Projectile	0.1640	0.0600	0.000309	4.8	260	9	15	0.15	90	90
4	60mm Mortar	0.2160	0.0600	0.000407	5	260	6	3	0.2	15	35
5	81mm Projectile	0.4260	0.0780	0.001357	5.2	260	11	2	0.3	50	65
6	105mm Projectile	0.4800	0.1050	0.002771	5.4	260	9	18	0.35	35	175
7	155mm Projectile	0.7000	0.1550	0.008806	5.2	260	16	10	0.45	45	135
8	175mm Projectile	0.8700	0.1750	0.013951	4.8	260	5	13	0.55	55	25
9	8in Projectile	0.8600	0.2030	0.018556	5.4	260	9	6	0.5	100	45
10	12in Projectile	1.2100	0.3040	0.058551	6.5	260	13	7	0.8	65	70
11	14in Projectile	1.4800	0.3560	0.098211	6.6	260	5	9	0.9	20	85
12	16in Projectile	1.6900	0.4060	0.145860	7.0	260	4	5	1.1	90	55
13	500lb Bomb	1.5900	0.2660	0.058906	4.1	260	14	15	1	80	40
14	750lb Bomb	1.2500	0.4060	0.107885	3.2	260	15	3	0.85	60	10
15	1,000lb Bomb	1.8400	0.3390	0.110717	4.2	260	4	16	1.2	70	90
16	2,000lb Bomb	2.5000	0.4570	0.273383	3.4	260	10	10	1.5	0	0

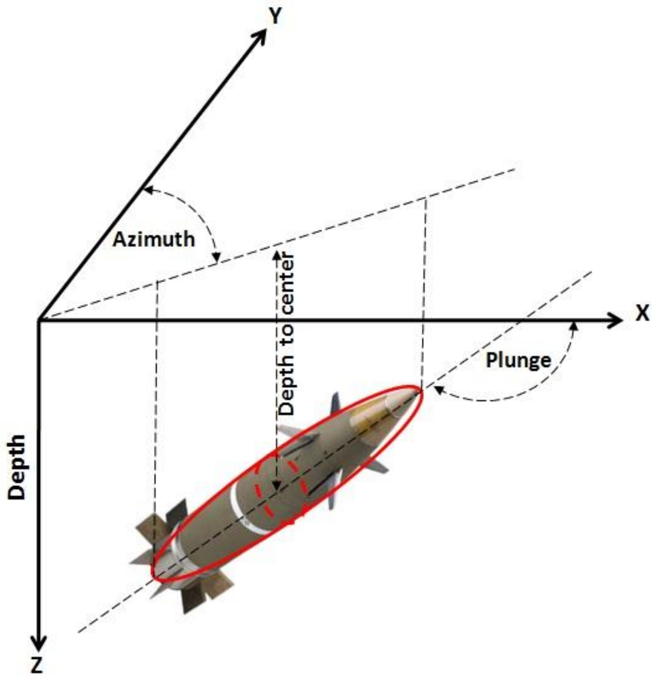

Figure 2. Simulation of UXO target with prolate spheroid.

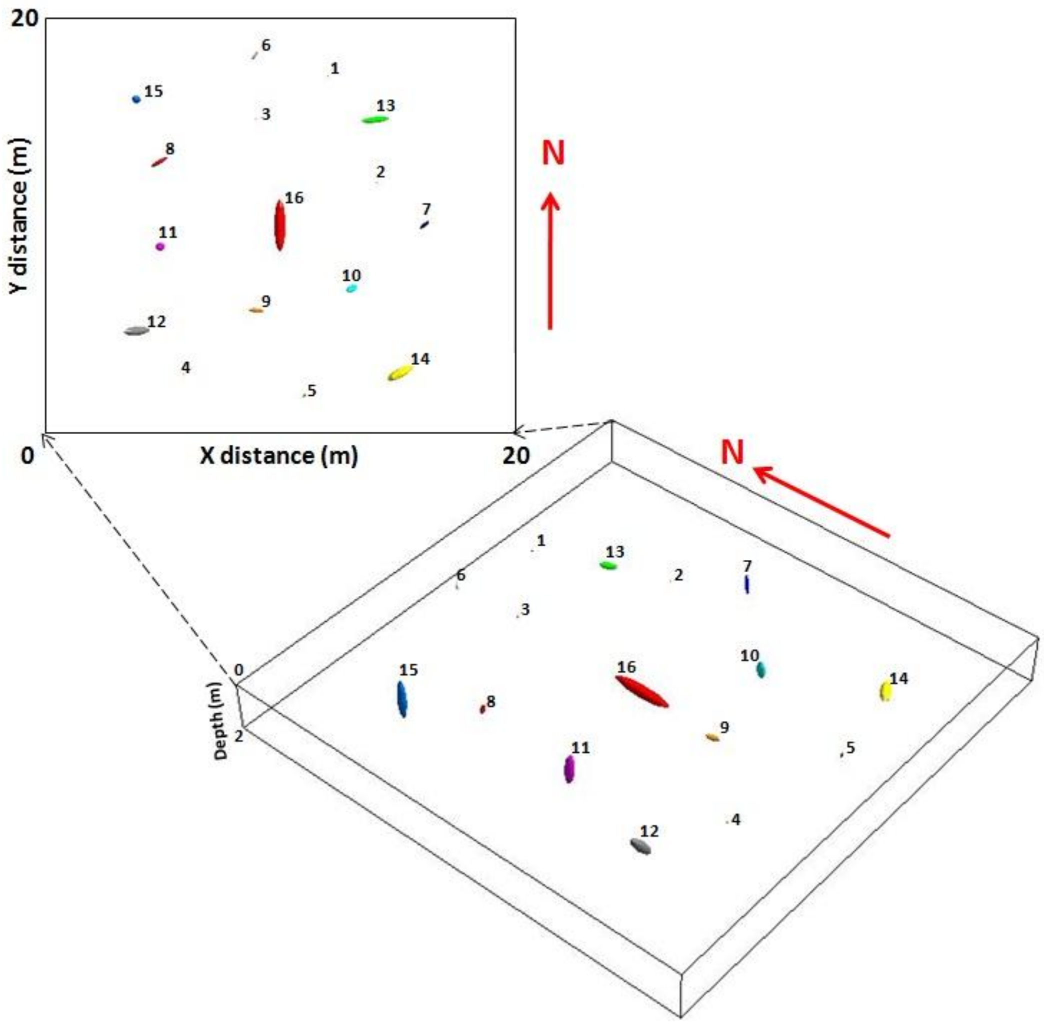

Figure 3. 3D & 2D plots of the synthetic UXO bodies in potential exploration.

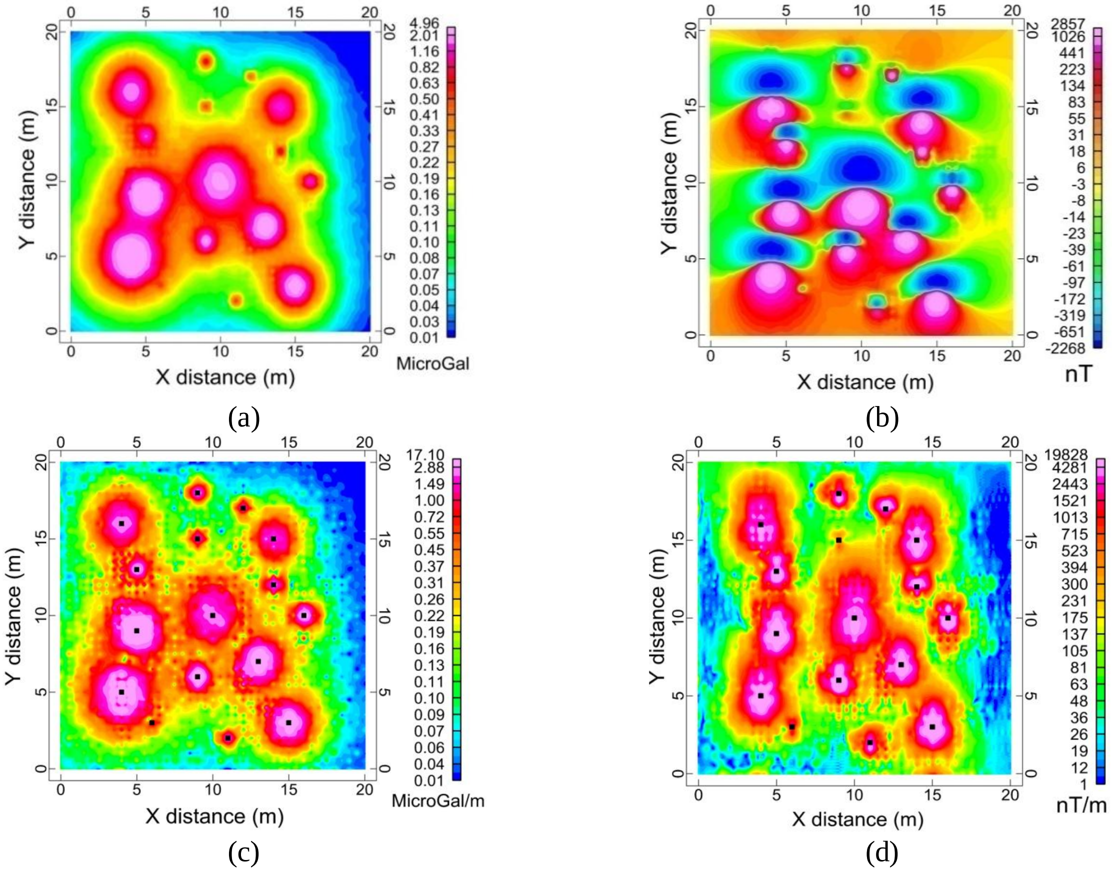

Figure 4. Synthetic potential field data, (a) gravity response, (b) magnetic response, (c) analytical signal map of the gravity response, (d) analytical signal map of the reduced-to-pole of the magnetic response. Both gravity and magnetic data are corrupted by 5% random Gaussian noise. The real locations of ordnance items are shown by filled box symbol superimposed on the analytic signal maps.

UXO is generally made of steel and whose typical susceptibility values range from several hundreds to over a thousand in international system of units (SI unit) [8, 46]. Here, it has been assumed a fixed susceptibility value of 260 in SI unit for all synthetic models (Table 1). Moreover, the inducing magnetic field is 46,000 nT with an inclination of 50° and declination of 3°. The remanence inclination and declination are also 60° and 10°, respectively. The demagnetization effect was computed as well. We assumed constant background value of 0.001 (SI unit) susceptibility and of 2.5 gr/cm^3 densities. The calculated magnetic and gravity responses were corrupted with a random Gaussian noise of 5% of data amplitude. Figures 4a and b shows the gravity and magnetic anomalies caused by assumed bodies respectively. The sample distance of the synthetic surveys is 0.5 m.

To enhance the locations of the synthetic bodies, the 3D analytic signal was applied for potential field anomalies. The outputs are shown in Figures 4c and d for gravity and magnetic data. The locations of assumed ordnance items are superimposed on Figures 4c and d with filled box symbol. It is obvious that these locations are at the center of the enhanced analytic signal outputs. It should be noted that enhancing high frequency noises in the maps generated by the analytic signal method which causes lots of picked locations using the Blakely algorithm. These unreal locations produce lots of false alarm sources in UXO detection that may be considered mistakenly as assumed UXO targets in synthetic potential field data. To suppress such a noise effect and to reduce the number of false alarms in the picked locations by Blakely algorithm, the surface gravity and magnetic data were upward continued at the altitudes of 0.25 and 0.3 m, respectively. Since the size of UXO targets are small (i.e. the weak amplitude of the observed potential field data), we have selected a low continuation height. The analytic signal maps of the upward continued data are shown respectively in Figures 5a and b while removing the effect of noise. For both Figures 4d and 4b, the analytic signal method was applied to the reduced-to-pole map of magnetic data to show better the real locations of causative sources.

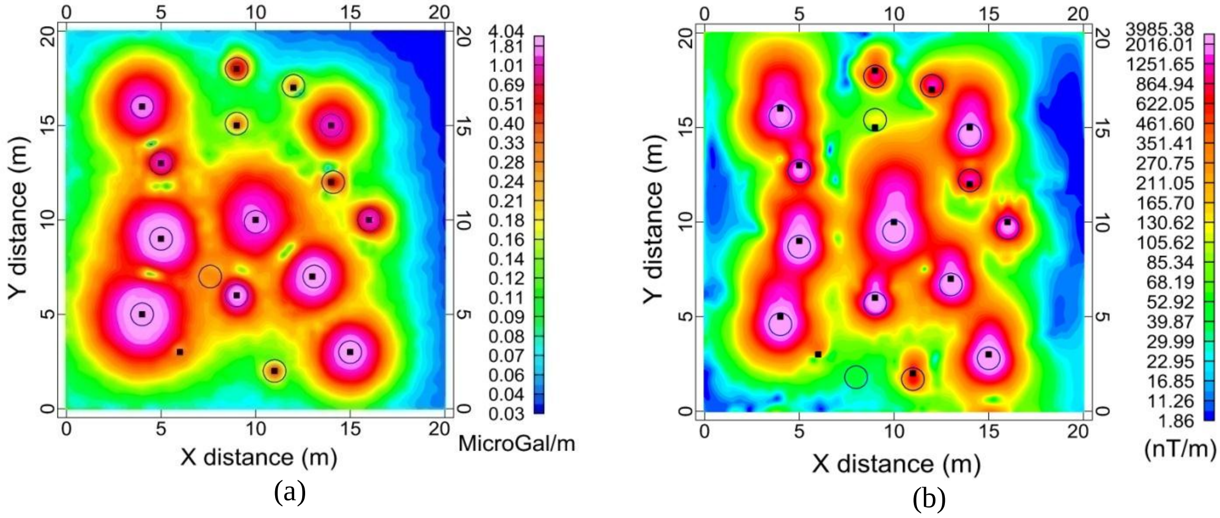

Figure 5. The Blakely results applied on the analytic signal maps of the upward continued potential data. (a) gravity, (b) magnetic. Gravity and magnetic data have been upward continued 0.25 and 0.30 m, respectively. The filled boxes show the real locations of the ordnance items while the picked locations by the Blakely algorithm are shown by circle symbol.

The automatic picking algorithm of the Blakely accompanying by the AN-EUL method were applied on both maps in Figures 5a and b on which the outputs are superimposed. The circle symbol shows the locations of picked sources by the Blakely algorithm. Except ordnance item 4, all items were picked in both gravity and magnetic map shown in Figures 5a and b. One item as a false alarm source for both data was selected which is related to no real location of items. Small ordnance item 4 since is located near to the bigger item 12, the automatic pick detection algorithm could not find it as an target. The AN-EUL method was applied on the picked anomalies of potential data to estimate the depth and the SI of causative sources. Tables 2 and 3 respectively shows the gravity and magnetic results. Generally from both Tables, the results show that the AN-EUL could approximately estimate the depth and the SI of ordnance items but it faces with problem in the parameter estimation of small ordnance items. Since such small items have lower response amplitude, the estimated depths are deeper than the true ones and subsequently it estimates higher SI values, which are out of the range of the assumed prolate spheroid SI. The prolate spheroid SI intervals are at (2 to 3) and (1 to 2) respectively for magnetic and gravity bodies.

Table 2. The results of the AN-EUL method applied on the synthetic gravity data which picked 15 out of 16 ordnance items by the automatic Blakely algorithm.

Obj. Num.	X Cor. (m)	X Cor. Estimation (m)	Y Cor. (m)	Y Cor. Estimation (m)	Depth from center (m)	Estimated Depth from top of model (m)	SI
1	12	12.00	17	17.10	0.06	1.31	>3
2	14	14.10	12	12.00	0.09	1.76	>3
3	9	9.00	15	15.01	0.15	5.05	>3
4	6	-	3	-	0.2	-	-
5	11	11.00	2	2.00	0.3	1.22	>3
6	9	9.00	18	18.00	0.35	0.50	2.79
7	16	16.00	10	10.00	0.45	0.5	2.10
8	5	5.00	13	13.00	0.55	0.44	1.71
9	9	9.00	6	6.00	0.5	0.34	1.49
10	13	13.10	7	7.00	0.8	0.45	1.01
11	5	5.00	9	9.00	0.9	0.47	0.66
12	4	4.00	5	5.00	1.1	0.06	<0.5
13	14	14.00	15	15.00	1	0.38	<0.5
14	15	15.00	3	3.00	0.85	0.54	0.92
15	4	4.00	16	16.00	1.2	0.47	0.64
16	10	10.00	10	9.90	1.5	1.24	1.21

Table 3. The results of the AN-EUL method applied on the synthetic magnetic data which picked 15 out of 16 ordnance items by the automatic Blakely algorithm.

Obj. Num.	X Cor. (m)	X Cor. Estimation (m)	Y Cor. (m)	Y Cor. Estimation (m)	Depth to center (m)	Estimated Depth from top of model (m)	SI
1	12	12.00	17	17.20	0.06	0.83	>4
2	14	14.00	12	12.20	0.09	0.83	>4
3	9	9.00	15	15.40	0.15	0.02	<0.5
4	6	-	3	-	0.2	-	-
5	11	11.00	2	1.70	0.3	0.91	>4
6	9	9.00	18	17.70	0.35	0.61	3.33
7	16	16.00	10	9.70	0.45	0.68	3.14
8	5	5.00	13	12.70	0.55	0.57	2.81
9	9	9.00	6	15.40	0.5	0.02	<0.5
10	13	13.00	7	6.70	0.8	0.53	1.73
11	5	5.00	9	8.70	0.9	0.65	1.78
12	4	4.00	5	4.60	1.1	0.67	1.46
13	14	14.00	15	14.60	1	0.62	1.46
14	15	15.00	3	2.80	0.85	0.85	2.43
15	4	4.00	16	15.60	1.2	0.21	<0.5
16	10	10.00	10	9.50	1.5	1.14	1.79

4. Real case studies

Two real case studies are considered here. The first one is a magnetic gradient survey provided by Barthel & Schriber GmbH, Cologne, Germany [47]. It forms part of a much larger dataset collected within Germany to detect UXO buried in the sediments of the Rhine River. The data was collected using a towed array of gradiometers with a sensor height of 0.55 m. The conducted survey has a sample interval along line of 10 cm, and 70 cm of line spacing. Figure 6a shows the magnetic gradiometry map. To suppress the effect of noise on observed data, 0.5-m upward continuation filter of the original data was applied. At first the Blakely algorithm was used to pick the probable UXO targets. Since lots of false alarms produce by this approach, the outputs of the AN-EUL method for selected picks were processed to remove unrealistic targets. The UXO SI locates at interval of (3 to 4) for magnetic gradiometry data; hence, we discarded the targets (picked previously by the Blakely algorithm) having the SI out of the interval of (2.5 to 5). This wider interval was selected because some estimated UXO's SI in synthetic modeling for the sake of noise effect, upward continuation and weak response located out of the desired interval. Here, the result shows finding of 20 UXO targets the estimated parameters of which are summarized in Table 4. The location plot of the picked UXO targets are shown in Figure 6b with circle symbol.

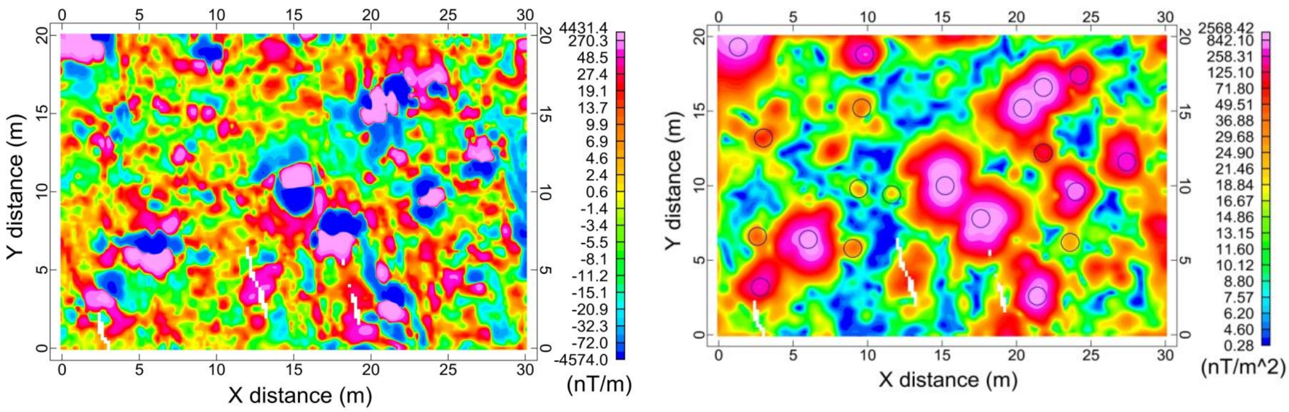

(a) (b)

Figure 6. Real magnetic case study, (a) the magnetic gradiometry map, (b) the picked targets by the Blakely algorithm superimposed on the analytical signal map of the 0.5-m upward continued data. The circle symbol shows the location of the picked targets.

Table 4. The results of the AN-EUL method applied on the real magnetic gradiometry data showing 20 picked UXO targets.

Obj. Num.	X Cor. (m)	Y Cor. (m)	Estimated Depth	SI
1	1.30	19.30	0.92	3.50
2	24.00	9.60	0.62	3.65
3	21.40	2.60	0.94	4.66
4	2.80	3.20	0.83	3.77
5	9.00	5.80	1.06	3.53
6	23.60	6.20	1.48	2.91
7	6.00	6.40	0.89	4.10
8	2.60	6.60	0.63	2.84
9	17.60	7.80	0.68	2.64
10	11.60	9.40	0.42	2.85
11	9.40	9.80	0.84	4.45
12	15.20	10.00	1.12	4.34
13	27.40	11.60	0.52	3.21
14	21.80	12.20	0.61	3.37
15	3.00	13.20	0.49	2.87
16	9.60	15.20	0.87	4.84
17	20.40	15.20	0.57	2.54
18	21.80	16.60	0.75	3.18
19	24.20	17.40	0.70	2.74
20	9.80	18.80	0.52	2.61

The second case study involves a gravity survey over an inert 155-mm projectile at a manmade test site. The 155-mm projectile, with 0.637-m length, 0.155-m diameter and 45.25-kg mass was buried in a horizontal orientation at 0.09-m depth to the top located at coordinates of x=1.5 m and y=1.5 m. The azimuth of the model with the north direction is 0° (N-S oriented). The survey area is 3×3 m and the measurement grid spacing is 0.5 m. The residual corrected gravity data over the projectile site is shown in Figure 7a. Relative to gravity reference value at coordinate (0, 0), most of the area of the survey grid is negative, except for a small positive area along the western boundary and a close positive anomaly approximately centered over the 155-mm projectile [3]. The range of relative gravity values over the area is approximately -14 to +7 μGal, for a maximum variation of 21 μGal. The observed data was upward continued 10 cm to suppress the effect of noise. The analytic signal map of the upward continued gravity data is shown in Figure 7b while applying the Blakely algorithm picked 5 targets. Two targets are over the projectile and three false alarms are also picked. The AN-EUL filtered results for estimated SI at interval (1 to 2) were shown in Table 5. The estimated depth and SI over the located projectile are in well agreement with the true ones. Here, the microgravity survey results successfully detected a positive anomaly over buried 155-projectile but the problem of false alarms still exist.

As a consequence, it was shown that the AN-EUL method could effectively reduce the number of false alarms which are mistakenly considered as UXO sources. After implementing the automatic picking algorithm, i.e. Blakely, and post processing method by AN-EUL, the false alarms are still high. Therefore, developing post processing algorithms to be applied on picked locations of probable UXO sources may decrease the effect of such issue in UXO detection.

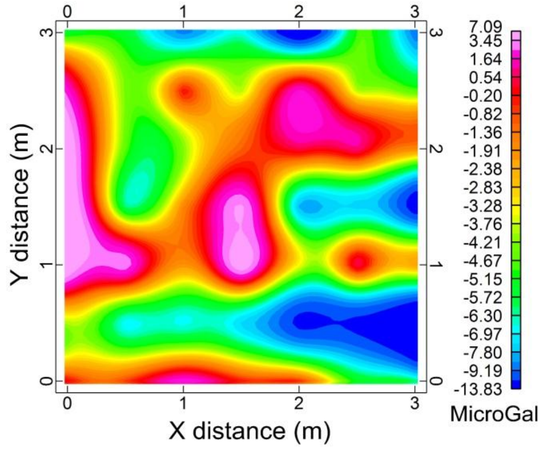

(a)

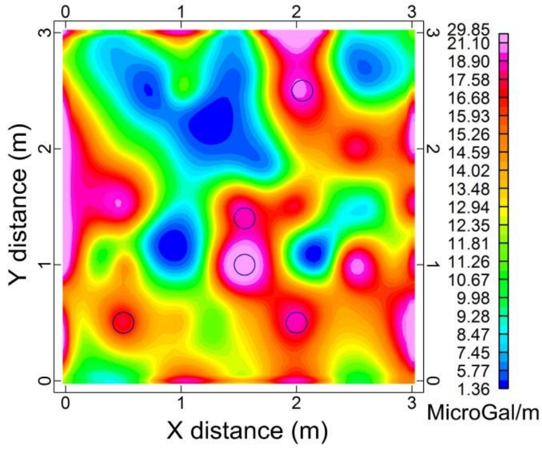

(b)

Figure 7. Real gravity case study, (a) the gravity map, (b) the picked targets by the Blakely algorithm superimposed on the analytical signal map of the gravity data. The circle symbol shows the location of the picked targets.

Table 5. The results of the AN-EUL method applied on the real gravity data showing 5 picked UXO targets.

Obj. Num.	X Cor. (m)	Y Cor. (m)	Estimated Depth	SI
1	0.50	0.50	0.26	1.09
2	2.00	0.50	0.43	1.86
3	1.55	1.00	0.12	1.32
4	1.55	1.40	0.15	1.40
5	2.05	2.50	0.29	1.02

5. Conclusions

This paper presented the application of potential field data in UXO detection. To detect the locations of the causative sources in potential exploration, the Blakely automatic picking algorithm was applied to select the locations of probable UXO targets. Since the algorithm is sensitive to noise level, many false alarms may be detected. To suppress such effect, the upward continued map can be effective in such cases. The results of applied AN-EUL method which simultaneously estimate the depth and the SI of picked targets showed its effectiveness in UXO detection. Estimated parameters of some small UXO sources also showed unrealistic results in synthetic modeling while their locations corresponded to the true ones. Based upon the estimated SI of the probable picked sources by automatic algorithm, a post-processing stage is needed to discard unrealistic sources which may highly increase the number of false alarms in UXO detection, and subsequently cause higher cost project.

Acknowledgments

The authors gratefully acknowledge the elite foundation office at the Malek Ashtar University of Technology, Tehran. We thank the College of Mining Engineering at the University of Tehran allowing the first author to do this project besides the PhD's thesis.

References

[1]. Pawlowski, J. (1994). Ordnance Investigation Using an Electromagnetic Method, Lake Erie, Port Clinton, Ohio, report for USAE Waterways Experiment Station, by Geophysics Ltd., Mississauga, Ontario.

[2]. Pawlowski, J., Lewis, R., Dobush, T. and Valleau, N. (1995). Proceeding of the Symposium on the Application of Geophysics to Engineering and Environmental Problems, Orlando, Florida, USA.

[3]. Butler, D.K. (2000). Assessment of Microgravity for UXO Detection and Discrimination. U.S. Army Engineer Research and Development Center: 1-37.

[4]. Butler, D.K. (2003). Implications of magnetic backgrounds for unexploded ordnance detection. Journal of Applied Geophysics, 54: 111-125.

[5]. Bell, T., Barrow, B., Miller, J. and Keiswetter, D. (2001). Time and Frequency Domain Electromagnetic Induction Signatures of Unexploded Ordnance. Subsurface Sensing Technology and Applications, 2: 153-175.

[6]. Beard, L.P., Doll, W.E., Holladay, J.S., Gamey, T.J., Lee, J.L.C. and Bell, D.T. (2004). Field tests of an experimental helicopter time-domain electromagnetic system for unexploded ordnance detection. Geophysics, 69: 664-673.

[7]. Pasion, L.R., Billings, S.D., Oldenburg, D.W. and Walker, S.E. (2007). Application of a library based method to time domain electromagnetic data for the identification of unexploded ordnance. Journal of Applied Geophysics, 61: 279-291.

[8]. Sanchez, V., Li, Y., Nabighian, M.N. and Wright, D.L. (2008). Numerical Modeling of Higher Order Magnetic Moments in UXO Discrimination. IEEE Trans. Geosci. Remote Sens., 46: 2568-2583.

[9]. Davis, K., Li, Y. and Nabighian, M. (2010). Automatic detection of UXO magnetic anomalies using extended Euler deconvolution. Geophysics, 75: G13-G20.

[10]. Davis, K., Li, Y. and Nabighian, M.N. (2011). Effects of low-pass filtering on the calculated structure index from magnetic data. Geophysics, 76: L23-L28.

[11]. Li, Y., Devriese, S.G.R. and Krahenbuhl, R.A. (2013). Enhancement of Magnetic Data by Stable Downward Continuation for UXO Application. IEEE Trans. Geosci. Remote Sens., 51: 3605-3614.

[12]. Pederson, A. and Stalcup, B. (1997). Phase III advanced technology demonstrations at Jefferson proving ground. Proceedings of the UXO Forum '97: pp. 281 – 289.

[13]. Bruschini, C., Gros, B., Guerne, F., Piéce, P.Y. and Carmona, O. (1998). Ground penetrating radar and imaging metal detector for antipersonnel mine detection. Journal of Applied Geophysics, 40: 59-71.

[14]. Huang, H. and Won, I.J. (2000). Conductivity and Susceptibility Mapping Using Broadband Electromagnetic Sensors. Journal of Environmental and Engineering Geophysics, 5: 31-41.

[15]. Huang, H. and Won, I.J. (2003). Characterization of UXO-Like Targets Using Broadband Electromagnetic Induction Sensors. IEEE Trans. Geosci. Remote Sens., 41: 652-663.

[16]. Huang, H. and Won, I.J. (2003). Detecting metal objects in magnetic environments using a broadband electromagnetic method. Geophysics, 68: 1877-1887.

[17]. Huang, H. and Won, I.J. (2003). Automatic anomaly picking from broadband electromagnetic data in an unexploded ordnance (UXO) survey. Geophysics, 68: 1870-1876.

[18]. Huang, H. and Won, I.J. (2004). Electromagnetic detection of buried metallic objects using quad-quad conductivity. Geophysics, 69: 1387-1393.

[19]. Huang, H., SanFilipo, B., Oren, A. and Won, I.J. (2007). Coaxial coil towed EMI sensor array for UXO detection and characterization. Journal of Applied Geophysics, 61: 217-226.

[20]. Koppenjan, S.K., Allen, C.M., Gardner, D., Wong, H.R., Lee, H. and Lockwood, S.J. (2000). Multi-frequency synthetic-aperture imaging with a lightweight ground penetrating radar system. Journal of Applied Geophysics, 43: 251-258.

[21]. Butler, D.K. (2001). Potential fields methods for location of unexploded ordnance. The Leading Edge, 20: 890 – 895.

[22]. Butler, D.K., Wolfe, P.J. and Hansen, R.O. (2001). Analytical modeling of magnetic and gravity signatures of unexploded ordnance. Journal of Environmental and Engineering Geophysics, 6: 33 – 46.

[23]. Butler, D.K., Simms, J.E., Furey, J.S. and Bennett, H.H. (2012). Review of Magnetic Modeling for UXO and Applications to Small Items and Close Distances. Journal of Environmental and Engineering Geophysics, 17: 53-73.

[24]. Benavides, A. and Everett, M.E. (2007). Non-linear inversion of controlled source multi-receiver electromagnetic induction data for unexploded ordnance using a continuation method. Journal of Applied Geophysics, 61: 243-253.

[25]. Billings, S.D. and Youmans, C. (2007). Experiences with unexploded ordnance discrimination using magnetometry at a live-site in Montana. Journal of Applied Geophysics, 61: 194-205.

[26]. Billings, S.D. and Wright, D. (2010). Interpretation of high-resolution low-altitude helicopter magnetometer surveys over sites contaminated with unexploded ordnance. Journal of Applied Geophysics, 72: 225-231.

[27]. Butler, D.K., Cespedes, E.R., Cox, C.B. and Wolfe, P.J. (1998). Multisensor methods for buried unexploded ordnance detection, discrimination, and identifications, Technical Report SERDP-98-10, US Army Engineer Waterways Experiment Station, Vicksburg, MS.

[28]. Butler, D., Cespedes, E., O'Neill, K., Arcone, S., Llopis, J., Curtis, J., Cullinane, J. and Meyer, C. (1998). Overview of science and technology program for JPG phase IV. Proceedings of the UXO Forum '98, Anaheim, CA.

[29]. Pasion, L.R. and Oldenburg, D.W. (2001). A discrimination algorithm for UXO using time domain electromagnetics. Journal of Engineering and Environmental Geophysics, 6: 91–102.

[30]. Keiswetter, D. (2000). Advances in frequency domain electromagnetic induction techniques for improved discrimination and identification of buried unexploded ordnance. Proceedings of the UXO/Countermine Forum 2000, Anaheim, CA.

[31]. Billings, S.D. (2004). Discrimination and classification of buried unexploded ordnance using magnetometry. IEEE Trans. Geosci. Remote Sens., 42: 1241-1251.

[32]. Billings, S.D. (2009). Field measurement of induced and remanent moments of unexploded ordnance and shrapnel. IEEE Trans. Geosci. Remote Sens., 47: 815-827.

[33]. Salem, A. and Ravat, D. (2003). A combined analytic signal and Euler method (AN-EUL) for automatic interpretation of magnetic data. Geophysics, 68: 1952-1961.

[34]. Blakely, R.J. and Simpson, R.W. (1986). Approximating edges of source bodies from magnetic or gravity anomalies. Geophysics, 51: 1494–1498.

[35]. Nabighian, M.N. (1972). The analytic signal of two-dimensional magnetic bodies with polygonal cross-section: its properties and use for automated anomaly interpretation. Geophysics, 37: 507–517.

[36]. Nabighian, M.N. (1974). Additional comments on the analytic signal of two dimensional magnetic bodies with polygonal cross-section. Geophysics, 39: 85–92.

[37]. Nabighian, M.N. (1984). Toward a three-dimensional automatic interpretation of potential field data via generalized Hilbert transforms: Fundamental relations. Geophysics, 49: 780–786.

[38]. Roest, W.R., Verhoef, J. and Pilkington, M. (1992). Magnetic interpretation using 3-D analytic signal. Geophysics, 57: 116-125.

[39]. Blakely, R.J. (1995). Potential theory in gravity and magnetic applications. Cambridge Univ. Press.

[40]. Debeglia, N. and Corpel, J. (1997). Automatic 3-D interpretation of potential field data using analytic signal derivatives. Geophysics, 62: 87-96.

[41]. Reid, A.B. (1995). Euler deconvolution: Past, present and future, a review: 65th Ann. Internat. Mtg., Soc. Expl. Geophys., Expanded Abstracts: 272–273.

[42]. Reid, A.B., Allsop, J.M., Granser, H., Millet, A.J. and Someron, I.W. (1990). Magnetic interpretation in three dimensions using Euler deconvolution. Geophysics, 55: 80-91.

[43]. Thompson, D.T. (1982). "EULDPH" A new technique for making computer-assisted depth estimates from magnetic data. Geophysics, 47: 31-37.

[44]. Hood, P. (1965). Gradient measurements in aeromagnetic surveying. Geophysics, 30: 891-902.

[45]. Ravat, D. (1996). Analysis of the Euler method and its applicability in environmental magnetic investigations. J. Environmental. Eng. Geophysics., 1: 229-238.

[46]. Billings, S.D, Pasion, C., Walker, S. and Beran, L. (2006). Magnetic models of unexploded ordnance. IEEE Trans. Geosci. Remote Sens., 44: 2115-2124.

[47]. Whitehead, N. (2007). Montaj UX-Detect^{TM}, Tutorial and User Guide. 105 p.

روش سیگنال تحلیلی- اویلر برای تفسیر اتوماتیک داده‌های پتانسیل جهت اکتشاف مهمات عمل‌نکرده

میثم عابدی[1*]، کیومرث موسی‌زاده[2]، حمید دهقانی[2]، احمد معدنچی‌زارع[2]

۱- دانشکده مهندسی معدن، دانشکده فنی، دانشگاه تهران، ایران

۲- دانشگاه صنعتی مالک اشتر، ایران

ارسال ۲۰۱۳/۹/۳، پذیرش ۲۰۱۴/۹/۶

* نویسنده مسئول مکاتبات: maysamabedi@ut.ac.ir

چکیده:

در این مطالعه روش تفسیر اتوماتیک داده‌های پتانسیل به نام سیگنال تحلیلی- اویلر در اکتشاف مهمات عمل‌نکرده بکار گرفته می‌شود که در حقیقت تلفیقی از رهیافت‌های سیگنال تحلیلی و دیکانولوشن اویلر است. این روش برای هر دو داده مغناطیس و گرانی و گرادیان آن‌ها بر مبنای مفهوم ضریب ساختاری بی‌هنجاری‌های پتانسیل که مرتبط با هندسه منابع بی‌هنجاری است قابل استفاده می‌باشد. با روش سیگنال تحلیلی- اویلر، عمق و هندسه تقریبی (ضریب ساختاری) منابع مولد قابل حصول است. یک مدل واقعی با شکل ساده برای شبیه‌سازی مهمات عمل‌نکرده، کروی کشیده است. روش سیگنال تحلیلی- اویلر بر روی داده‌های ساختگی پتانسیل (گرانی و مغناطیس) حاصل از شبیه‌سازی یک مجموعه از منابع مولد مهمات عمل‌نکرده با اندازه‌های متنوع در اعماق متفاوت بکار گرفته شد. برای هر دو داده، پارامترهای تخمینی عمق و ضریب ساختاری مهمات ساختگی تقریباً مطابق با پارامترهای مدل ساختگی بودند. شناسایی محل منابع مولد بر اساس الگوریتم اتوماتیک انتخاب محل بلکلی است. برای هر دو مجموعه داده ازآنجایی‌که پاسخ‌های بی‌هنجاری مهمات کوچک متأثر از نوفه است، ضریب ساختاری تخمینی تا حدودی تحت تأثیر قرار گرفته ولی محل آن‌ها منطبق بر واقعیت است. الگوریتم بلکلی همچنین بی‌هنجاری‌های ضعیفی که مرتبط با نوفه می‌باشند را شناسایی می‌نماید، بنابراین ممکن است، پردازش ضریب ساختاری تخمینی منابع اتوماتیک شناسایی‌شده مورد نیاز باشد تا از تولید آلارم‌های غلط در اکتشاف مهمات عمل‌نکرده جلوگیری شود. دو داده واقعی نیز تهیه شد تا توانایی روش در شناسایی مهمات عمل‌نکرده ارزیابی شود.

کلمات کلیدی: داده‌های پتانسیل، اکتشاف مهمات عمل‌نکرده، روش سیگنال تحلیلی- اویلر، الگوریتم بلکلی، تفسیر اتوماتیک.